KI REPORTS
KIReports.org
CLINICAL RESEARCH

Kidney Transcriptome Sequencing Improves Molecular Diagnosis and Reveals Splicing Complexity Across the Alport Spectrum

Jerica Pleško[1], Špela Kert[1], Sara Petrin[1], Špela Borštnar[2,3], Željka Večerić Haler[2,3], Anamarija Meglič[4], Nejc Piko[5], Alenka Matjašič[1], Nika Kojc[1] and Andrej Zupan[1]

[1]Faculty of Medicine, Institute of Pathology, University of Ljubljana, Ljubljana, Slovenia; [2]Clinical Department of Nephrology, University Clinical Center Ljubljana, Ljubljana, Slovenia; [3]Faculty of Medicine, University of Ljubljana, Ljubljana, Slovenia; [4]Nephrology Department, University Children's Hospital, University Medical Center, Ljubljana, Slovenia; and [5]Department of Dialysis, University Clinical Center Maribor, Maribor, Slovenia

Introduction: Hereditary glomerular basement membrane (GBM) disorders caused by pathogenic variants in *COL4A3/A4/A5* are increasingly recognized as Alport spectrum. Disease severity varies widely and is influenced by variant type, allelic dosage, sex, and genetic modifiers. DNA-based testing incompletely captures this heterogeneity, particularly splice-altering and regulatory variants, limiting precise molecular diagnosis and prognostic stratification.

Methods: We performed whole-transcriptome sequencing on 93 kidney biopsies from 93 patients (90 families) with ultrastructural GBM abnormalities. RNA-derived variant detection, splicing analysis, and gene expression profiling were integrated with histopathology, electron microscopy, and clinical data. Aberrant splicing events were quantified, and differential gene expression and microRNA (miRNA) motif enrichment analyses assessed molecular changes associated with kidney function decline.

Results: Transcriptome sequencing identified 64 pathogenic or likely pathogenic variants, including 14 splice-altering variants (22%), often involving noncanonical events, whose functional consequences are not readily resolved by routine DNA sequencing alone. Pathogenic or likely pathogenic variants were detected in 52 of 93 patients (56%), including novel missense and splice-altering variants in *COL4A3*, *COL4A4*, *COL4A5*, and *CLCN5*. Quantitative splicing revealed heterogeneous exon 27 skipping in *COL4A4*, indicating regulated exon usage. Gene expression profiling showed progressive estimated glomerular filtration rate (eGFR)-associated remodeling with activation of inflammatory and profibrotic pathways and suppression of renal transporter genes. miRNA enrichment implicated miR-335-5p, miR-325-3p, and miR-874-3p as potential regulators.

Conclusion: Kidney transcriptome sequencing improves molecular diagnosis across the Alport spectrum, enables interpretation of splice-altering variants, and captures signatures linked to progression. Integrating RNA-based analysis may refine classification, enhance prognostic assessment, and support precision medicine in hereditary nephropathies.

Kidney Int Rep (2026) **11,** 106710; https://doi.org/10.1016/j.ekir.2026.106710
KEYWORDS: Alport spectrum; COL4A4 exon 27 skipping; glomerular basement membrane; kidney transcriptomics; RNA sequencing; splicing variants

Alport syndrome (AS) is a hereditary kidney disease caused by pathogenic variants in the *COL4A3-5* genes, which encode the α3, α4, and α5 chains of type IV collagen. These proteins are essential components of the GBM and their disruption results in progressive renal pathology often accompanied by hearing loss and ocular abnormalities.[1] Historically, the diagnosis and classification of AS have been dichotomous, distinguishing "classic" AS from isolated benign hematuria or "thin basement membrane nephropathy (TBMN)", based on clinical severity.[2] However, this binary classification fails to reflect the full phenotypic and genotypic heterogeneity associated with *COL4A3-5* variants. In response to this

Correspondence: Andrej Zupan, Institute of Pathology, Faculty of Medicine, University of Ljubljana, Korytkova 2, 1000 Ljubljana, Slovenia. E-mail: andrej.zupan@mf.uni-lj.si; or, Nika Kojc, Institute of Pathology, Faculty of Medicine, University of Ljubljana, Korytkova 2, 1000 Ljubljana, Slovenia. E-mail: nika.kojc@mf.uni-lj.si

Received 25 February 2026; revised 30 June 2026; accepted 14 July 2026; published online 21 July 2026

limitation, a 2025 consensus led by Savige *et al*. proposed the term "Alport spectrum" to encompass the continuum of clinical presentations associated with these variants, from isolated microscopic hematuria to progressive kidney failure with extrarenal manifestations.[3] In line with the updated nomenclature, the autosomal dominant form is now recognized as the most prevalent type of AS, affecting at least 1 in 100 individuals. This is followed by the X-linked form, with an estimated prevalence of 1 in 2000, whereas digenic and autosomal recessive forms remain rarer. AS can be occasionally misdiagnosed as other conditions with overlapping clinical features, particularly those associated with variants in genes such as *COL4A1*, *LMX1B*, *MYH9*, or *CLCN5*.[3,4]

Advances in genomic technologies have highlighted the importance of transcript-level resolution for understanding the functional consequences of genetic variants in *COL4A3-5* genes. In particular, aberrant splicing events, ranging from exon skipping and cryptic splice site usage to intron retention and cryptic exons are increasingly implicated in the pathogenesis of Alport spectrum.[5,6] Conventional DNA-based diagnostics can detect many coding and near-splicing variants, but often do not fully resolve the functional consequences of splice-altering variants, particularly those in noncanonical splice regions, deep intronic sequences, or regulatory elements.[7] Transcriptome sequencing (RNA-seq) is a powerful approach for detecting aberrant splicing and quantifying differential transcript usage in a tissue-specific manner.[8] Although RNA analysis from cells of urinary sediment and blood has provided some insights, kidney-specific expression patterns remain inadequately captured because of the limited accessibility of renal tissue. Recent studies employing transcriptomic profiling of kidney biopsies or single-nucleus RNA-seq from archived samples have demonstrated the feasibility and diagnostic value of transcript-level analysis in nephrogenetic disorders, including AS.[9] Importantly, aberrant splicing events may serve as biomarkers for therapeutic targets. Antisense oligonucleotide-mediated splice correction, for example, holds promise in preclinical models of genetic kidney disease.[10] Integrating transcriptome sequencing into clinical pipelines for individuals with suspected Alport spectrum disorders may therefore improve diagnostic yield and reveal novel disease mechanisms.

However, transcriptome sequencing has not yet been broadly applied to large cohorts of patients with Alport spectrum to connect genetic variants with their transcript-level consequences and markers of disease progression, a gap that limits precise molecular diagnosis and therapeutic discovery. To address this, we used whole transcriptome sequencing of kidney biopsies to characterize the splicing landscape of Alport-associated genes, identify pathogenic variants directly from RNA, examine gene expression changes linked to eGFR decline and explore post-transcriptional regulatory networks through miRNA motif enrichment. The aims of this study were as follows: to (i) improve molecular diagnosis by detecting splice defects and pathogenic variants from RNA-seq; (ii) elucidate transcript-level disease mechanisms; (iii) characterize gene expression signatures associated with kidney function decline; and (iv) identify regulatory miRNA networks involved in disease progression.

Using whole transcriptome sequencing data from 93 kidney biopsies, we provide an integrated transcriptional and variant analysis that enhances diagnostic yield and reveals molecular signatures relevant to disease progression and potential therapeutic targeting.

METHODS

Study Design and Participants

This retrospective study included 93 archived fresh-frozen kidney biopsy samples obtained between 2012 and 2023 from adult and pediatric patients evaluated at tertiary referral centers. Patients diagnosed with AS based on genetic testing alone (genetic-first diagnosis) and patients (with advanced renal failure) who would not undergo biopsy were not included in this study. The primary inclusion criterion was the presence of ultrastructural GBM abnormalities identified by electron microscopy, consistent with disorders across the Alport spectrum. TBMN was defined by diffuse GBM thinning according to standardized thickness criteria, whereas AS was diagnosed in cases showing characteristic GBM thickening and multilamellation ("basket-weave" appearance) in conjunction with clinical findings. Patients presented with isolated GBM abnormalities or in combination with other renal pathologies. Exclusion criteria comprised transplant kidney biopsies, zero-hour biopsies, diabetic nephropathy, and IgA nephropathy. Clinical data, including age, sex, family history, hematuria, proteinuria, serum creatinine, and eGFR, were retrospectively retrieved from medical records (Supplementary Table S1). The study was conducted in accordance with the Declaration of Helsinki and approved by the Republic of Slovenia National Medical Ethics Committee (approval number 0120-466/2020/10). Informed consent for genetic analysis was obtained from all participants.

Clinical Outcome Analyses

Kidney survival was estimated using the Kaplan-Meier method, with end-stage kidney disease (ESKD) defined as the event. Patients who had not reached ESKD at the time of last follow-up were censored at their age at last clinical visit. Longitudinal kidney function trajectories were constructed using serial measurements of eGFR and serum creatinine obtained during routine follow-up. For each patient, values were aligned by age at measurement, and analyses were restricted to individuals with at least 2 available measurements per parameter.

Renal Histopathology

Kidney biopsies were evaluated using light microscopy, immunofluorescence, and electron microscopy as part of routine renal pathology diagnostics. The extent of global and segmental glomerulosclerosis and the degree of interstitial fibrosis and tubular atrophy (IFTA) were assessed semiquantitatively. Electron microscopy focused on evaluation of GBM ultrastructure, including thickness and multilamellation. GBM thickness was assessed according to established methodology, with the mean GBM thickness per glomerulus determined from measurements of randomly selected capillary loops.

RNA Sequencing and Variant Detection

Total RNA was extracted from frozen kidney tissue obtained by needle biopsy and assessed for integrity before library preparation. Strand-specific whole-transcriptome libraries were prepared and sequenced using Illumina (Illumina, San Diego, CA) platforms. RNA sequencing data were processed using standardized bioinformatic pipelines for quality control, alignment, variant calling, splicing analysis, and gene expression profiling.

Variants were detected directly from RNA sequencing data and annotated using curated kidney disease gene panels. Variant interpretation followed the American College of Medical Genetics and Genomics and Association for Molecular Pathology guidelines. *In silico* prediction tools were used to support assessment of missense and splice-altering variants.

Splicing, Gene Expression, and miRNA Analyses

Alternative splicing events were identified and quantified using junction-based methods, enabling calculation of percent spliced-in (Ψ) values on a per-sample basis. Aberrant splicing events were prioritized based on consistency across samples and predicted functional impact, and selected events were validated by reverse transcription polymerase chain reaction followed by Sanger sequencing.

Differential gene expression analysis was performed by stratifying patients according to eGFR ($\geq$ 60 vs. $<$ 60 ml/min per 1.73 m^2). Genes associated with renal injury, fibrosis, inflammation, and tubular transport were examined, and expression patterns were visualized using hierarchical clustering and heatmap analysis. miRNA target enrichment analysis was conducted using differentially expressed genes to identify candidate regulatory miRNAs.

Orthogonal DNA Validation

RNA-derived variants were validated using targeted DNA sequencing from peripheral blood, with additional Sanger sequencing performed where required. Copy number variation analysis was conducted using targeted sequencing data. Continuous variables are reported as medians with ranges. Statistical analyses were performed using standard survival and longitudinal approaches, with a 2-sided P-value < 0.05 considered statistically significant.

This study was reported in accordance with the Minimum Information about a High-Throughput Sequencing Experiment guidelines. A completed Minimum Information about a High-Throughput Sequencing Experiment guidelines checklist is provided as Supplementary Material.

Detailed experimental protocols and bioinformatics workflows are provided in the Supplemental Methods.

Assessment of Aberrant Splicing Events in Normal Kidney Samples

To assess whether selected splicing events are specific to disease, targeted analyses were performed in the control group consisted of 30 preimplantation (zero-time) kidney biopsy samples from kidney donors (9 females and 21 males) with a mean age of 48 years, characterized by minimal histopathological changes, an ultrastructurally normal GBM, and a favorable 1-year clinical course after transplantation. For these samples, all detected exon skipping events were evaluated and semiquantified using reverse transcription polymerase chain reaction, agarose electrophoresis, and Sanger sequencing.

RESULTS

Clinical Features and Histopathologic Findings

The study cohort comprised 93 individuals (38 males and 55 females) from 90 unrelated families. Based on ultrastructural and clinical criteria, 20 patients were diagnosed with AS and 73 with TBMN. In 67 patients, GBM abnormalities represented the primary ultrastructural finding, whereas in 26 patients GBM

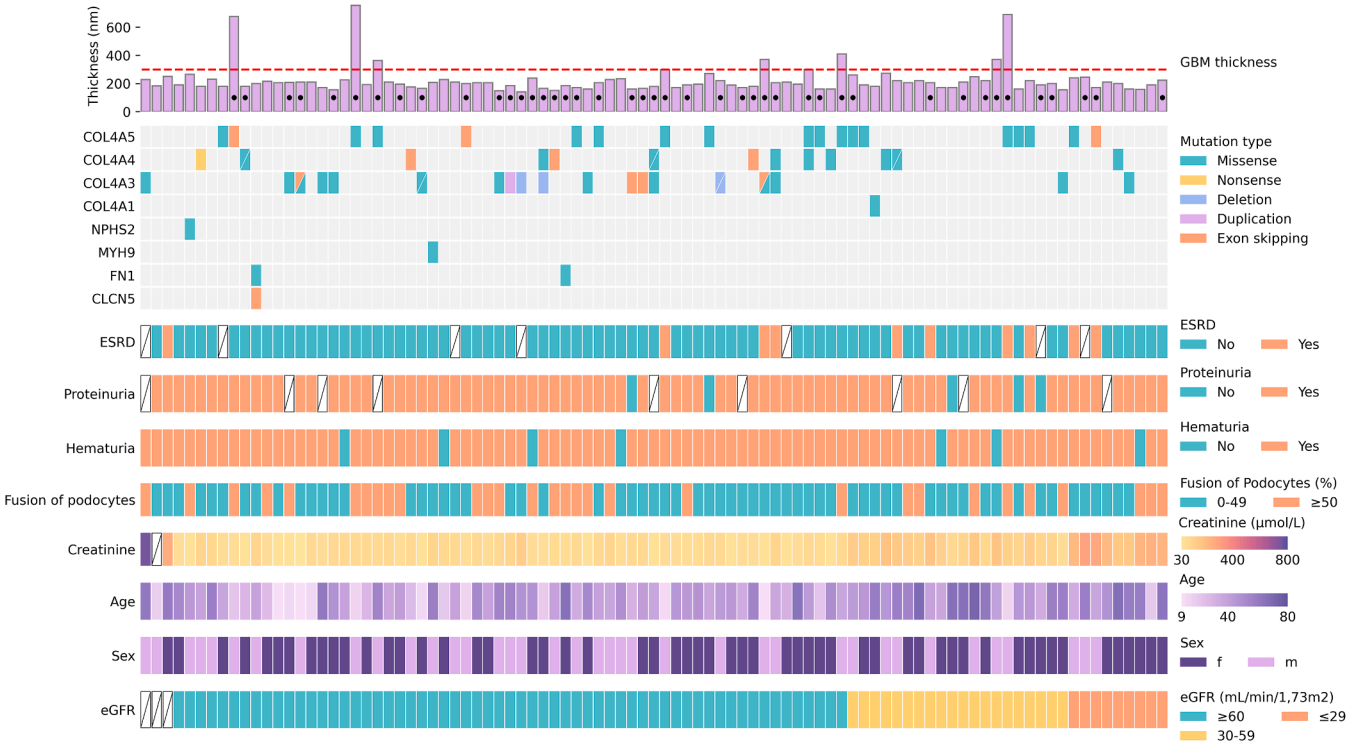

Figure 1. CoMut plot showing integrated analysis of GBM thickness, genetic variants, and clinical parameters in patients with suspected Alport spectrum disorders. The top panel shows the glomerular basement membrane (GBM) thickness for each sample (purple bars), with a dashed red line indicating the 350 nm diagnostic threshold and black dots indicating the presence of multilamellation. Below, the genetic variant landscape of key genes (*COL4A5*, *COL4A4*, *COL4A3*, *COL4A1*, *NPHS2*, *MYH9*, *FN1*, *CLCN5*) is displayed by variant type. Bottom annotations include the following clinical features: end stage renal disease (ESRD), proteinuria, hematuria, degree of podocyte foot process effacement, age, sex and estimated glomerular filtration rate (eGFR).

changes were observed as secondary findings in biopsies performed for other renal indications.

Renal biopsy was performed most frequently for chronic nephritic syndrome (44%), followed by hematuria with proteinuria (27%), nephrotic syndrome (9%), isolated proteinuria (9%), isolated hematuria (7%), suspected vasculitis (3%), and acute kidney injury (1%) (Figure 1; Supplementary Table S1). The median age at biopsy was 47 years (range: 9–79). Hematuria and proteinuria were present in 91.4% and 92.9% of patients, respectively, with proteinuria ranging from mild to nephrotic (median: 1.22 g/24 h). Median eGFR at biopsy was 81 ml/min per 1.73 m^2 (range: 17–162), and serum creatinine 85 µmol/l (range: 33–780).

During follow-up, 10 patients (10.8%) progressed to ESKD, requiring dialysis or kidney transplantation. Bilateral sensorineural hearing loss was documented in 26.3% of patients, and 47.3% reported a positive family history of renal disease. Kaplan–Meier analysis demonstrated a gradual, age-dependent decline in kidney survival, with approximately 70% of patients remaining free from ESKD at 30 years, 40% at 50 years, and fewer than 10% beyond 70 years of age (Supplementary Figure S1).

Histopathologic findings spanned a broad spectrum (Figure 1; Supplementary Table S1). Global glomerulosclerosis ranged from 0% to 90%, segmental glomerulosclerosis from 0% to 31%, and IFTA was mild in most cases but moderate to severe in patients with reduced eGFR. Electron microscopy revealed variable GBM thickening and irregularity, with thickness measurements ranging from 140 to 755 nm (median: 200 nm). GBM multilamellation was absent or mild in most biopsies but moderate or severe in approximately 13% of cases, predominantly among patients with advanced renal disease. Greater degrees of glomerulosclerosis, IFTA, and GBM multilamellation were observed in patients with X-linked hemizygous or autosomal biallelic variants, whereas milder changes predominated in individuals with heterozygous or hypomorphic variants.

Overview of Identified Variants

Whole transcriptome sequencing identified at least 1 variant in 52 of 93 patients (56.0%), yielding a total of 64 variants classified as pathogenic ($n = 28$), likely pathogenic ($n = 19$), or variants of uncertain significance ($n = 17$) (Supplementary Table S2). Most variants

Table 1. Summary of variant types identified by whole transcriptome sequencing across collagen-related and glomerulopathy-associated genes

Variant type	*COL4A3*	*COL4A4*	*COL4A5*	*COL4A1*	*FN1*	*MYH9*	*NPHS2*	*CLCN5*
Deletion (6.3%)	4	0	0	0	0	0	0	0
Duplication (1.6%)	1	0	0	0	0	0	0	0
Missense (73.4%)	14	12	16	1	2	1	1	0
Nonsense (1.6%)	0	1	0	0	0	0	0	0
Splice (17.2%)	4	3	3	0	0	0	0	1
N= 64	23	16	19	1	2	1	1	1

The table shows the number of deletion, duplication, missense, nonsense, and splice site variants detected in each gene. *COL4A3*, *COL4A4* and *COL4A5* harbored the majority of the variants. The total number of variants ($N = 64$) is indicated.

occurred in *COL4A3* ($n = 23$), *COL4A5* ($n = 19$), and *COL4A4* ($n = 15$), with additional variants identified in *COL4A1*, *CLCN5*, *FN1*, *MYH9*, and *NPHS2* (Figure 1; Table 1). Previous DNA-based genetic testing was performed using the same approach as described for the orthogonal DNA validation. Previous genetic testing results were available for 57 of 64 identified variants (89%). Among these, 48 variants (84%) had been previously detected at the DNA level, whereas 9 variants (16%) were either not detected or not reported (Supplementary Table S2).

Several variants were detected in multiple individuals, most notably *COL4A5* r.1871g>a (c.1871G>A, p.Gly624Asp), identified in 9 patients. Multiple previously unreported variants were identified, including missense, in-frame deletion, nonsense, and RNA-confirmed splice-altering variants absent from population databases and classified as pathogenic or likely pathogenic (Table 2).

Missense variants represented the most frequent variant type overall (73.4%), followed by splice-site variants (17.2%; Figure 2). However, among pathogenic and likely pathogenic variants, splice-altering variants accounted for a higher proportion (23.4%), highlighting their increased clinical relevance. Of the 11 splice-site variants, 5 affected canonical splice donor or acceptor sites, whereas 6 involved noncanonical or deep intronic regions or lacked a clearly identifiable genomic origin. Most missense variants involved glycine substitutions within the collagenous domain, consistent with established pathogenic mechanisms in collagen IV-related disorders. Of 47 missense variants, 34 (72.3%) had Rare Exome Variant Ensemble Learner scores > 0.7, supporting deleterious impact, and most variants were absent or extremely rare in population databases (Supplementary Table S2).

All splice-altering variants were classified as pathogenic under American College of Medical Genetics guidelines, fulfilling the Pathogenic Very Strong 1(RNA) criterion because of RNA-confirmed aberrant splicing. Aberrant splicing events were detected in *COL4A3*, *COL4A4*, *COL4A5*, and *CLCN5* (Figure 3; Table 3). Canonical splice-site variants were associated with high SpliceAI (Illumina, San Diego, CA) scores, whereas several noncanonical intronic variants exhibited moderate or low SpliceAI scores but nevertheless resulted in clear exon skipping at the RNA level. Notably, exon 44 skipping in *COL4A4* was detected without an identifiable DNA variant, suggesting a cryptic or deep intronic regulatory mechanism.

Phenotype-Genotype Correlations

Male patients with *COL4A5* variants, particularly those involving canonical glycine substitutions or exon-skipping events, exhibited the most severe

Table 2. Previously unreported pathogenic and likely pathogenic variants identified in *COL4A3*, *COL4A4*, *COL4A5*, and *CLCN5*

Gene (RefSeq)	RNA variant	DNA variant	Predicted protein variant	gnomAD	REVEL	Classification (ACMG)
COL4A3 (NM_000091.5)	r.2524g>c	c.2524G>C	p.(Gly842Arg)	0.0	0.924	Likely Pathogenic (PM1_Strong, PM2_Supp, PP3)
	r.2937_2945del	c.2937_2945del	p.(Lys984_Leu986del)	0.0	n/a	Likely Pathogenic (PM2_Supp, PM4, PM1_Strong)
COL4A4 (NM_000092.5)	r.4091_4216del (exon 44 skipping)	*not detected*	p.(Glu1365_Gly1406del)	n/a	n/a	Pathogenic (PVS1(RNA), PM2_Supp, PM1_Strong)
COL4A5 (NM_033380.3)	r.359g>c	c.359G>C	p.(Gly120Ala)	0.0	0.94	Likely Pathogenic (PP3, PM2_Supp, PM1_Strong, PM5)
	r.466_546del (exon 9 skipping)	c.466-17T>G	p.(Glu157_Gly183del)	0.0	n/a	Pathogenic (PVS1(RNA), PM2_Supp, PM1_Strong)
	r.4824_4983del (exon 52 skipping)	c.4804-15C>A	p.(Glu1608Aspfs*6)	0.0	n/a	Pathogenic (PVS1(RNA), PM2_Supp, PM1_Strong)
CLCN5 (NM_001127898.4)	r.416_603del (exon 7 skipping)	c.603G>A	p.(Ala142Cysfs*38)	0.0	n/a	Likely Pathogenic (PVS1(RNA), PM2_Supp,)

ACMG, American College of Medical Genetics and Genomics; gnomAD, genome aggregation database; PVS1, pathogenic very strong 1; REVEL, rare exome variant ensemble learner. All variants were classified based on ACMG criteria, supported by in silico predictions (REVEL) and absence or rarity in the gnomAD population database.

phenotypes, characterized by early-onset hematuria and proteinuria, rapid decline in renal function, and frequent progression to ESKD during the second to fourth decades of life (Supplementary Table S1). Longitudinal serum creatinine trajectories stratified by gene and inheritance pattern demonstrated substantial interindividual variability (Figure 4; Supplementary Figures S2–S3). Patients with *COL4A5* variants showed the steepest increases in creatinine, often beginning in adolescence or early adulthood.

Individuals with *COL4A3* or *COL4A4* variants generally exhibited slower progression, although biallelic variants were associated with markedly accelerated renal decline. Patients whose creatinine exceeded 500 μmol/l were predominantly within the X-linked group, with the exception of 1 patient carrying a *COL4A3* exon 34 skipping variant accompanied by an additional *COL4A3* variants of uncertain significance. Longitudinal eGFR trajectories paralleled creatinine-based findings, with X-linked and autosomal recessive cases showing steeper declines and earlier progression to ESKD (Supplemental Figures S4–S6).

In contrast, carriers of the hypomorphic *COL4A5* p.(Gly624Asp) variant demonstrated a milder disease course, with preserved renal function into mid-adulthood, slower eGFR decline, and fewer extrarenal manifestations, underscoring the influence of variant-specific effects on clinical outcome.

The patient carrying the *CLCN5* exon 7 skipping variant presented with persistent microscopic hematuria and mixed subnephrotic proteinuria (∼2 g/d), with both glomerular and tubular components. Hypercalciuria was not detected, although renal ultrasound revealed microlithiasis. Kidney function was moderately impaired, with a serum creatinine of approximately 120 μmol/l and an eGFR of 63 ml/min per 1.73 m^2. Kidney biopsy performed in 2017 demonstrated TBMN with 50% global glomerulosclerosis and 20% IFTA, whereas an earlier biopsy from 1999 had already shown TBMN.

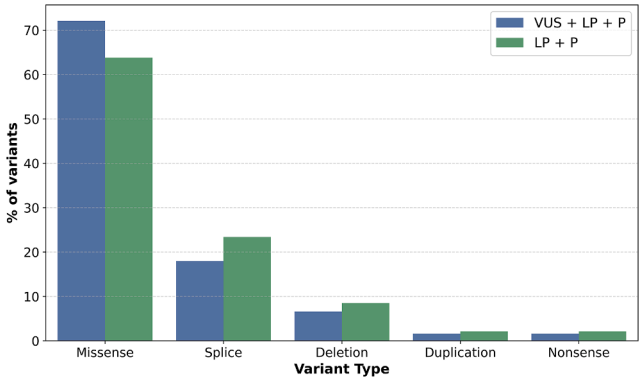

Figure 2. Frequency of detected variant types. Barplot showing the relative percentage of each variant type among all detected variants classified as either a variant of unknown significance (VUS) + Likely Pathogenic (LP) + Pathogenic (P) (blue) or Likely Pathogenic + Pathogenic (LP + P) (green). Missense variants represent the majority in both groups but the relative proportion of splice site variants increases when focusing solely on pathogenic or likely pathogenic variants.

Variable Splicing of COL4A4 Exon 27

Quantitative splicing analysis revealed heterogeneous exon 27 skipping in *COL4A4* across most samples (Figure 5). The mean exon inclusion level was 0.869 (median: 0.879; range: 0.659–0.992), with partial exon exclusion observed in a large subset of samples. These findings indicate that exon 27 is predominantly retained but subject to variable, context-dependent alternative splicing, even in the absence of pathogenic variants.

Validation and Segregation Analyses

All RNA-derived variants were successfully validated at the genomic DNA level using targeted sequencing, with the exception of *CLCN5*, which was confirmed by Sanger sequencing. No copy number variations were detected. Segregation analysis of the *CLCN5* exon 7 skipping event (Figure 6) confirmed its presence in an affected sibling, supporting familial segregation of the splicing defect. All aberrant splicing events identified by RNA sequencing were validated by Sanger sequencing, except for *COL4A4* exon 20 skipping, which was attributable to a known genomic deletion.

All candidate splicing defects were semi-quantitatively assessed in a cohort of 30 preimplantation kidney biopsy samples from kidney donors. Targeted evaluation demonstrated that 2 exon-skipping events are also present in nondiseased tissue. In particular, *COL4A4* exon 27 skipping was consistently observed across samples, with variable exon inclusion levels (approximately 20–80%), indicating heterogeneous alternative splicing. In contrast, *COL4A5* exon 52 skipping was absent or detected in normal kidney samples only at lower levels, with 2 exceptions (Supplementary Table S3).

Differential Gene Expression and miRNA Enrichment Analyses

Differential gene expression analysis comparing patients with preserved (eGFR ≥ 60 ml/min per 1.73 m^2) and reduced kidney function revealed distinct transcriptional signatures associated with disease progression (Figure 7). Samples were clustered according to eGFR strata, demonstrating progressive upregulation of genes related to renal injury, fibrosis, and inflammation with declining kidney function. Injury markers such as *HAVCR1*, *LCN2*, and *SPAG5* were markedly

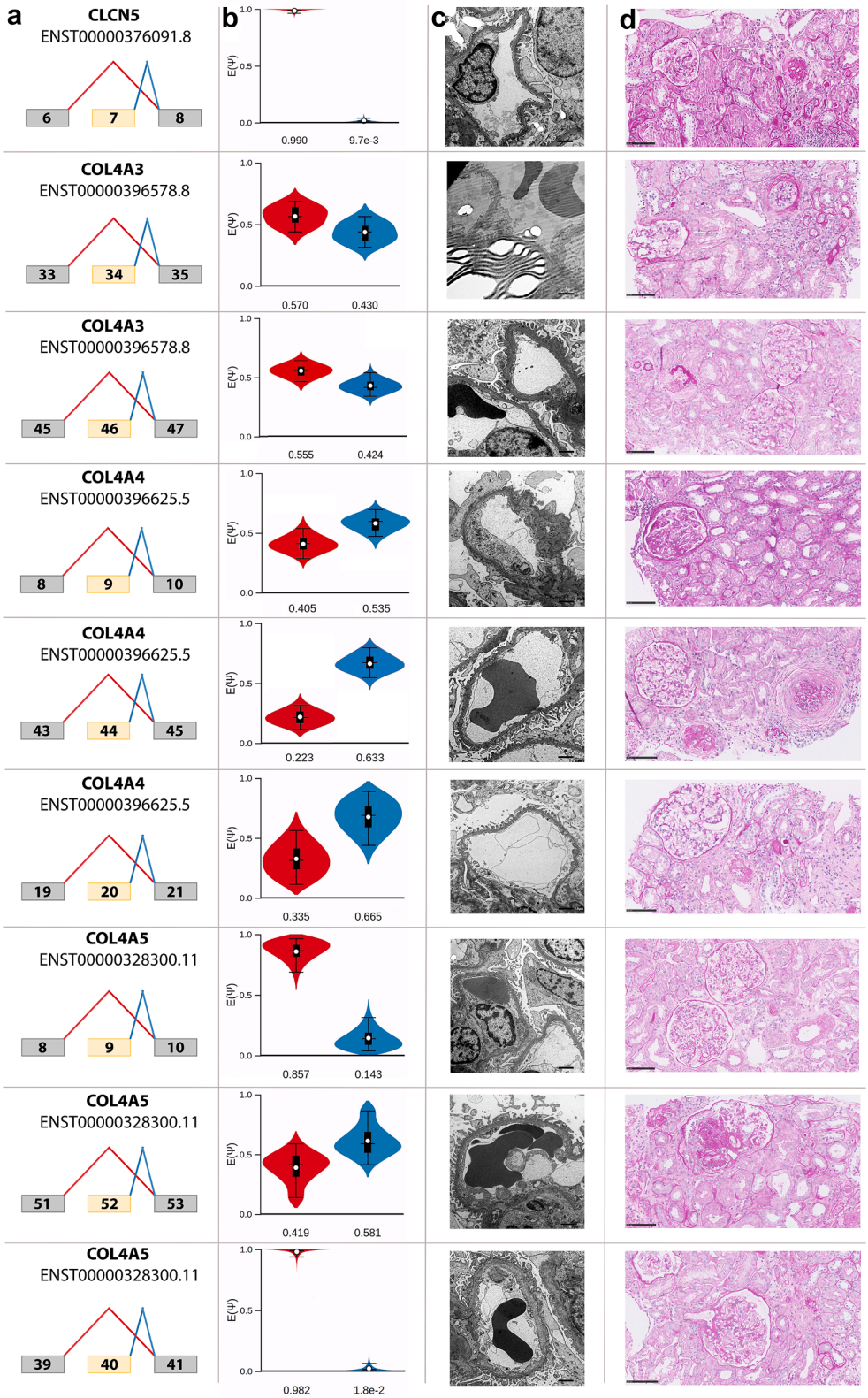

Figure 3. Molecular and histopathological findings in selected cases demonstrating exon skipping and structural alterations in glomerular basement membrane disease. (a, b) Exon-skipping events detected in kidney biopsies. The left panels depict alternative splicing events with different exon inclusion levels (red as retaining and blue as a skipping event). The right panels show violin plots representing splicing event distribution (red as retaining and blue as a skipping event). (c) Electron microscopy (EM) reveals irregular thickening and multilamellation of the glomerular basement membrane (GBM) indicative of Alport spectrum (original magnification, 2500X). (d) Segmental and global glomerulosclerosis, along with interstitial fibrosis and tubular atrophy, represent common chronic histopathological changes observed during the progression of Alport spectrum disorders.

Table 3. Aberrant splicing events detected by whole transcriptome sequencing and their corresponding variants identified by targeted DNA sequencing

Gene (RefSeq)	Aberrant splicing event	DNA variant (HGVS)	Aggregate SpliceAI	gnomAD
CLCN5 (NM_001127898.4)	Exon 7 skipping	c.603G>A	0.77	0.0
COL4A3 (NM_000091.5)	Exon 34 skipping	c.2881+1G>A	0.72	0.0
	Exon 46 skipping	c.4028-15T>C	0.24	0.00000137
COL4A4 (NM_000092.5)	Exon 9 skipping	c.559-2A>T	0.99	0.00000137
	Exon 44 skipping	*Not detected*	n/a	n/a
	Exon 20 skipping	c.1321_1369+3del	1.00	0.00000205
COL4A5 (NM_033380.3)	Exon 40 skipping	c.3588A>G	0.05	0.0
	Exon 52 skipping	c.4804-15C>A	0.09	0.0
	Exon 9 skipping	c.466-17T>G	0.50	0.0

gnomAD, genome aggregation database; HGVS, Human Genome Variation Society.
Listed are the affected genes, transcript IDs, types of splicing abnormalities, associated DNA variants, SpliceAI aggregate scores and allele frequencies from the gnomAD database. SpliceAI scores ≥ 0.5 suggest a strong prediction (high precision) of splicing impact. "Not detected" indicates no matching DNA variant was found for the observed transcript event.

upregulated in severe disease. Fibrosis-associated genes, including *COL1A1*, *COL3A1*, and *FN1*, showed increased expression, consistent with extracellular matrix remodeling. Inflammatory mediators and *TNF* receptor family members were also upregulated in moderate to severe disease stages.

Conversely, genes involved in tubular transport and epithelial function (*SLC22A6*, *AQP1*, *UMOD*) were progressively downregulated with declining eGFR, reflecting loss of tubular integrity. miRNA enrichment analysis identified several miRNAs predicted to regulate differentially expressed genes, including hsa-miR-335-5p, hsa-miR-325-3p, and hsa-miR-874-3p, whereas enrichment among downregulated gene sets did not reach statistical significance (Table 4).

DISCUSSION

In this cohort of 93 kidney biopsies with ultrastructural GBM abnormalities, kidney tissue whole transcriptome sequencing improved molecular diagnosis and enhanced insight into the Alport spectrum. By integrating RNA-based variant detection, splicing analysis, and expression profiling, we identified previously unreported pathogenic splice and missense variants and revealed gene expression changes associated with declining kidney function. These data illustrate that RNA sequencing of disease-relevant tissue is a powerful complement to DNA-based diagnostics, revealing splicing defects and regulatory events that underlie phenotypic diversity in collagen

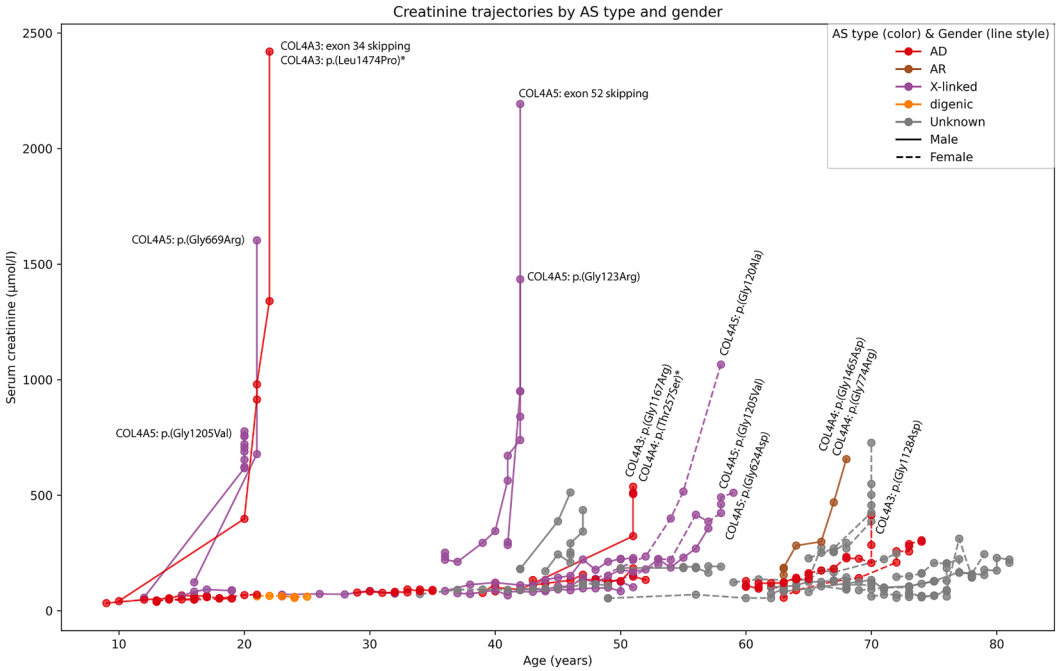

Figure 4. Longitudinal creatinine trajectories in Alport spectrum by mode of inheritance type and gender. Serum creatinine values from all clinical visits were plotted for each patient and colored by mode of inheritance (AD, AR, X-linked, digenic or unknown). Solid and dashed lines represent male and female patients, respectively. Peak trajectories are annotated with the corresponding variants. An asterisk (*) indicates variants classified as VUS.

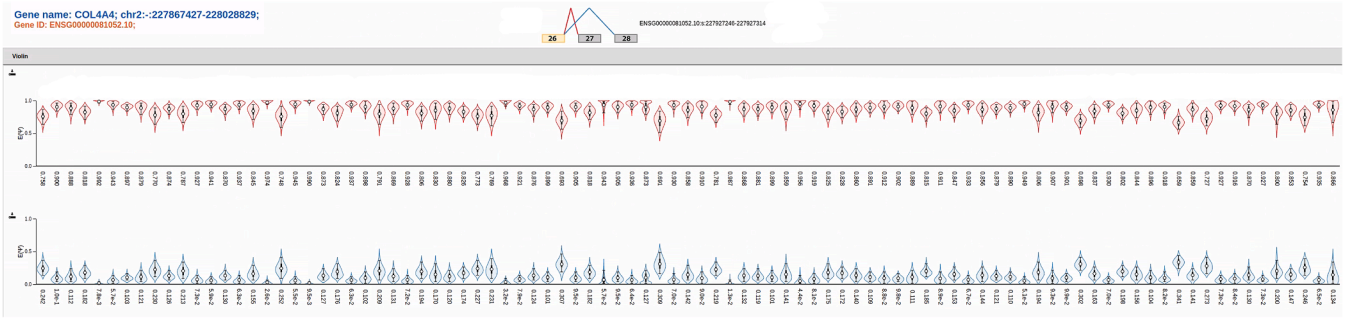

Figure 5. Variable levels of exon 27 skipping in *COL4A4* transcript (NM_000092.5) across kidney samples. Violin plots depicting differential inclusion of exon 27 in *COL4A4* transcripts across the analyzed kidney samples. The upper panel (red) represents exon inclusion levels (mean: 0.869), whereas the lower panel (blue) illustrates exon skipping events (mean: 0.131), quantified using RNA-seq derived percent spliced-in (Ψ) values. Each violin corresponds to a single sample, with distribution width reflecting variability in exon usage. The observed variation in exon 27 skipping indicates heterogeneous alternative splicing of *COL4A4*, potentially affecting α4(IV) collagen chain production and the structural integrity of the glomerular basement membrane.

IV–related nephropathies, however broader splicing variability must be interpreted with caution.

Variant Spectrum and Genotype-Phenotype Correlations

Overall, we identified 64 variants with pathogenic, likely pathogenic or variants of uncertain significance classification involving *COL4A3* – *COL4A5* and additional genes associated with GBM nephropathy. Seven pathogenic and/or likely pathogenic variants appear to be novel, since they had not been reported in the literature or public genetic databases. Most of these variants were associated with renal function deterioration, including progression to ESKD. Histopathologically, the majority of cases showed a relatively high proportion of global glomerulosclerosis, accompanied by segmental glomerulosclerosis and a substantial degree of IFTA. Ultrastructural examination most frequently demonstrated GBM thinning, with absent or mild multilamellation; severe multilamellation was observed in only 2 cases. The most frequent variant identified in our cohort was *COL4A5* p.(Gly624Asp), detected in 9 individuals (9.7%). This recurrent variant represents a founder genetic variant in Central and Eastern Europe, including the Balkan region.[11] It substitutes a conserved glycine within the collagen IV α5 triple-helix domain but behaves as a hypomorphic allele, leading to a milder clinical phenotype.[11–13] However, in our cohort, affected individuals exhibited relatively advanced histopathological changes, including global glomerulosclerosis, segmental glomerulosclerosis, and moderate to severe IFTA, accompanied by pronounced ultrastructural GBM abnormalities. Additionally, deterioration of renal function was observed in 2 of 9 patients. Despite extensive sequencing, therefore, establishing robust genotype–phenotype correlations within the Alport spectrum remains challenging. The complexity arises from heterogeneous genetic backgrounds, the presence of hypomorphic alleles and the likely contribution of additional genetic modifiers influencing disease severity. Analysis of longitudinal creatinine and eGFR trajectories corroborates previous observations of pronounced interindividual variability, with some patients maintaining isolated hematuria throughout life, whereas others progress to ESKD in early adulthood. Overall, our results indicate that X-linked inheritance in males is associated with more severe disease, whereas autosomal dominant forms are generally milder, consistent with previous studies.[14] However, in certain autosomal dominant cases, the presence of an additional variant of

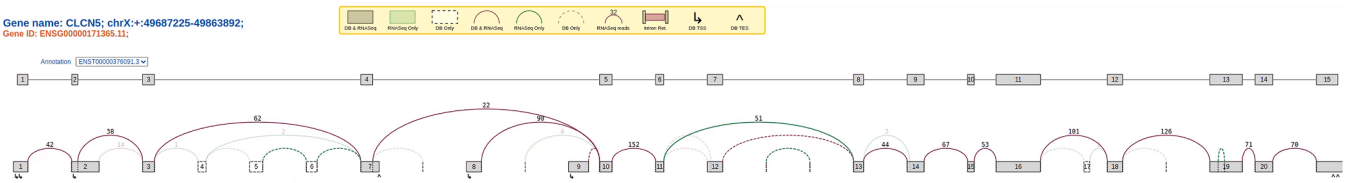

Figure 6. Exon 7 skipping in the *CLCN5* transcript (NM_001127898.4). Schematic representation of alternative splicing in the *CLCN5* transcript located on chromosome X. Exon 7 skipping is indicated by an absent junction between exons 6 and 7, with a direct splicing event connecting exon 6 to exon 8 (green arc). The arc diagram below the exon map displays the splicing junctions detected from RNA-seq reads (green arcs) and database plus RNA-seq annotations (purple arcs). The observed skipping event results in the exclusion of exon 7 from the mature transcript.

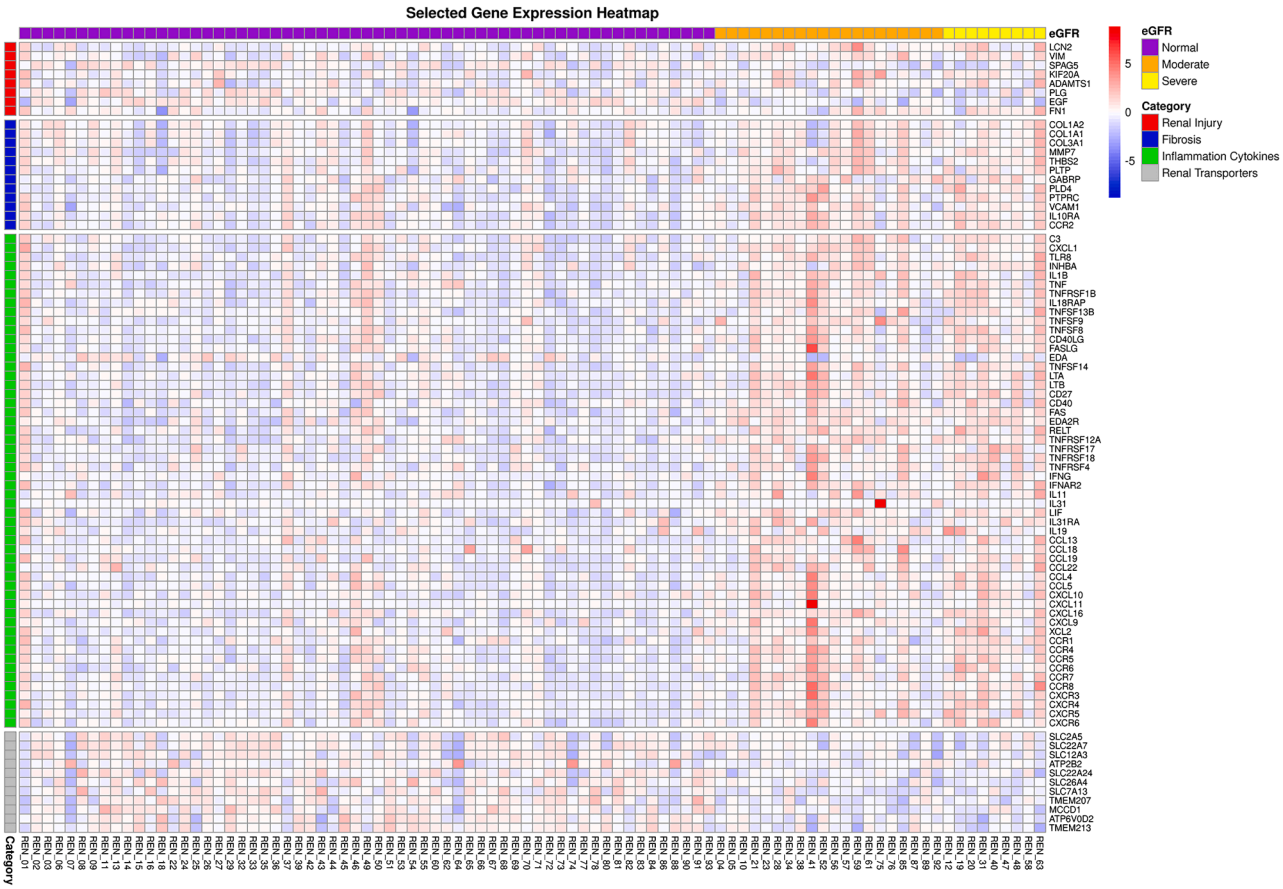

Figure 7. Selected gene expression heatmap of kidney tissue samples stratified by eGFR status. Differential gene expression analysis was performed between two groups defined by eGFR status: normal renal function and reduced renal function. For visualization purposes only, samples within the reduced renal function group were further annotated as moderate or severe impairment based on eGFR values (top annotation bar). Genes are categorized by biological function: renal injury (blue), fibrosis (brown), inflammation (green), and renal transporters (grey). Red indicates upregulation and blue indicates downregulation (Z-score scaled). A progressive increase in injury, fibrosis, and inflammatory markers, along with reduced transporter expression, is observed with worsening renal function.

uncertain significance may modify the phenotype, resulting in an autosomal recessive-like clinical presentation. An illustrative example from our cohort is *COL4A3* p.(Leu1474Pro), which, when present alongside a *COL4A3* exon-skipping variant, was associated with a severe AS phenotype, including moderate GBM ultrastructural abnormalities and progression to ESKD. The p.(Leu1474Pro) substitution occurs in the NC1 domain of collagen IV and has been described as a putative hypomorphic allele rather than a fully penetrant pathogenic variant.[14] Given its incomplete penetrance and relatively high allele frequency in the general population, accurate risk stratification for carriers should incorporate clinical findings, such as proteinuria and GBM ultrastructural features, rather than relying on the genetic variant alone.

Splicing Heterogeneity and Functional Interpretation

Splice-altering variants accounted for over one-fifth of pathogenic findings, highlighting the major contribution of aberrant splicing to disease pathogenesis. Importantly, many canonical splice-site and near-splice variants can be detected by routine diagnostic approaches, such as targeted gene panels or exome sequencing. However, noncanonical splice-region, deep-intronic, or regulatory variants are more difficult to interpret, and their pathogenicity often cannot be established confidently without transcript-level evidence.[15–20] In our cohort, RNA sequencing of kidney tissue enabled direct confirmation of aberrant exon usage and helped resolve the functional significance of splice defects that might otherwise remain classified as variants of uncertain significance or even likely benign variants. For 1 exon skipping event (*COL4A4* exon 44 skipping), we did not detect the causative variant, implying deep intronic or regulatory variants outside capture boundaries, or structural and/or allelic mechanisms not captured by standard panels. These findings emphasize that the major strength of our study lies in the transcriptome-first analysis of disease-relevant tissue.

Table 4. miRNAs enriched for targets among differentially expressed genes in kidney tissue, identified using enrichMiR

Regulation	miRNA	Log_2 (enrichment)	FDR	DEG groups	Binding site collection
Downregulated	hsa-miR-5691	2.33	0.255	Normal egfr vs. low egfr	miRTarBase
	hsa-miR-6805-3p	2.33	0.255	Normal egfr vs. low egfr	miRTarBase
	hsa-miR-5004-3p	2.66	0.698	Normal egfr vs. low egfr	miRTarBase
Upregulated	hsa-miR-335-5p	0.52	0.000513	normal eGFR vs. low eGFR	miRTarBase
	hsa-miR-325-3p	0.76	0.000083	Normal eGFR vs. low eGFR	Target scan conserved
	hsa-miR-874-3p	1.13	0.0472	Normal eGFR vs. low eGFR	Target scan conserved

DEG, differentially expressed genes; FDR, false discovery rates.
The table lists predicted up- and down-regulated miRNAs with target enrichment based on the miRTarBase or TargetScan (conserved) binding site collections. Shown are log_2 (enrichment) values, FDR, and corresponding DEG group comparisons.

The tissue-based approach is particularly important in hereditary nephropathies. Although RNA from peripheral blood, urinary sediment, or skin fibroblasts may sometimes be informative, expression of kidney disease genes and splice isoforms may be low or not fully representative in this surrogate tissues. In addition, formalin-fixed paraffin-embedded kidney biopsies are generally not suitable for comprehensive RNA studies of this type. By analyzing the fresh-frozen tissue of interest directly, we were able to assess the transcriptomic consequences of suspected disease-causing variants in the tissue of interest itself.

An interesting finding of our study was variable *COL4A4* exon 27 skipping across the majority of kidney samples. Quantitative differences in exon inclusion (mean 87%) and exclusion (mean 13%) indicate that this event might represent a regulated alternative splicing process rather than a pathogenic defect, which is further supported by the fact that this event was observed broadly also in normal kidney tissue. However, no alternative transcript with skipped exon 27 is reported in Genotype-Tissue Expression database. Increasing evidence indicates that not all exon-skipping events are inherently pathogenic and that their clinical relevance depends on both the quantitative ratio between normal and aberrant transcripts and the functional context of the affected gene.[19,21-23] Although exon 27 skipping appears to be benign computationally,[4] our recent study demonstrated that a high level of aberrant transcript in combination with a second skipping event can lead to severe autosomal recessive AS.[24] In many cases, variants located outside canonical splice sites result in "leaky" splicing defects, whereby a fraction of transcripts are correctly spliced whereas others exhibit partial exon skipping, intron retention, or activation of cryptic splice sites.[25] Such events can yield a mixture of normal and abnormal transcripts and the proportion of correctly spliced transcripts can determine whether sufficient protein function is retained to prevent a clinical phenotype.[26,27] Although exon 27 skipping in *COL4A4* was *in vitro* validated as being disruptive for a heterotrimeric assembly of collagen IV chains,[28] its pathogenicity interpretation should be case-dependent, considering the quantitative nature of this skipping event.

The low-level detection of *COL4A5* exon 52 skipping in normal kidney biopsy samples may reflect the presence of a minor alternative transcript (ENST00000644079.1), which comprises only 3 exons and has been reported in public transcriptomic datasets (Genotype-Tissue Expression). However, in our patient, exon 52 skipping was dominant (90%), strongly supporting a pathogenic splicing defect rather than physiological alternative splicing. However, since higher proportion of exon 52 skipping was also observed in 2 normal controls, further functional validations are required in order to assess the full nature of this transcriptomic event.

Novel Splice Disruption in *CLCN5* and Phenotypic Convergence

We identified a novel exon 7 skipping event in *CLCN5* associated with GBM thinning and hematuria in the absence of classical Dent disease features. Segregation analysis confirmed the presence of the same splicing defect in an affected sibling, supporting its pathogenic relevance. Although this finding supports pathogenicity at the molecular level, its relationship to the observed renal phenotype requires careful interpretation. *CLCN5* variants are associated with Dent disease, a disorder of proximal tubular function characterized by low-molecular-weight proteinuria, hypercalciuria, and nephrolithiasis. In this context, it remains unclear how *CLCN5* dysfunction would directly result in basement membrane thinning. However increasing evidence indicates phenotypic overlap between tubular and glomerular disorders, including Alport-like presentations.[29-31] Variants identified in genes beyond the classical *COL4A3-COL4A5* spectrum, further emphasize the growing recognition of phenocopies in hereditary nephropathies. Increasing evidence demonstrates that Alport-like clinical and histopathological features may arise from genetically distinct disorders, complicating diagnostic classification and highlighting the limitations of phenotype-based approaches alone. Recent studies have shown that a substantial proportion of patients with suspected AS harbor pathogenic variants in alternative genes, underscoring the importance of broad genetic testing strategies and careful molecular

interpretation.[32,33] In parallel, the traditional view of AS as a primarily glomerular disease is being refined. Emerging data suggest that the tubular compartment plays a more significant role in disease pathogenesis and progression than previously appreciated. Recent work by Loderbauer *et al*.[34] provides initial evidence supporting a role for tubular involvement in AS, indicating that tubular dysfunction may contribute to disease progression alongside GBM defect. This concept is consistent with our findings of progressive downregulation of tubular transporters and activation of injury and inflammatory pathways with declining kidney function.

Transcriptomic Remodeling Across Kidney Function Decline

Expression profiles of kidney tissue reflect the clinical severity of renal dysfunction and chronic injury burden. As eGFR declined, we observed a progressive upregulation of genes associated with renal inflammatory and profibrotic pathways, alongside a coordinated downregulation of genes encoding renal transporters. These changes are broadly consistent with transcriptomic patterns reported across many forms of chronic kidney disease and should not be interpreted as specific molecular mechanisms of the Alport spectrum alone. Rather, they likely represent shared downstream response to progressive kidney injury. The pattern we identified is consistent with trajectory analyses in large kidney transcriptomic datasets, in which worsening kidney function is accompanied by increasing activation of proinflammatory cytokine signaling (e.g., *IL6*, *TNF*, and *NF-κB* pathways), extracellular matrix remodeling and *TGF-β* driven fibrotic gene programs, coupled with suppression of proximal tubular transporters (e.g., *SLC34A1*, *SLC5A2*, and ATPases) and mitochondrial oxidative phosphorylation genes.[35-40] Single-nucleus and single-cell RNA-seq studies of human kidney disease further corroborate these findings, showing that even within the same nephron segment, subsets of tubular cells follow distinct transcriptional trajectories, from an intact, transport-competent state toward inflammatory and fibrotic fates. The relative abundance of these maladaptive cell states correlates strongly with histologic injury and eGFR decline.[37,39,41-43] Such single-cell analyses have revealed that chronic injury induces a loss of epithelial identity and a gain in proinflammatory and profibrotic signaling, thereby amplifying interstitial fibrosis and tubular atrophy. Together, these data support a model in which tubular dedifferentiation and inflammatory activation are central features of progressive kidney injury, independent of the primary etiology. The concordance of our data with previous bulk and single-nucleus transcriptomic studies suggests that eGFR-linked gene expression changes can serve as robust molecular readouts of kidney health and injury burden.

miRNA Regulatory Networks and Molecular Adaptation

The miRNA motif enrichment analysis in our study implicated miR-335-5p, miR-325-3p, and miR-874-3p among upregulated miRNAs, when comparing low versus normal eGFR patients groups. Although motif enrichment does not establish causality, previous functional work supports an anti-inflammatory and/or antifibrotic role for miR-325-3p in diabetic nephropathy via chemokine C-C motif ligand 19 targeting,[44] warranting targeted validation in renal cell models. miR-335-5p has been implicated in the regulation of fibrotic and inflammatory signaling across multiple tissues, including the kidney. In tubular epithelial cells, it attenuates TGF-β1 induced epithelial-mesenchymal transition and collagen synthesis by suppressing downstream effectors, such as *ADAM19* and *ROCK1*, thereby preserving epithelial integrity and limiting fibrosis.[45,46] Its upregulation in patients with reduced eGFR may thus reflect a compensatory antifibrotic response to chronic renal injury. miR-874-3p has been implicated in renal oxidative stress and apoptotic injury, in which its overexpression amplifies mitochondrial dysfunction and cell death pathways. In doxorubicin-induced nephrotoxicity, miR-874-3p directly targets MsrB3, a mitochondrial antioxidant enzyme, thereby enhancing reactive oxygen species accumulation and podocyte apoptosis.[47] Its upregulation in our low-eGFR group may thus represent a maladaptive component of tubular injury, contributing to oxidative stress–driven loss of cellular integrity. Together, these miRNAs delineate a complex regulatory landscape, where both adaptive and maladaptive responses coexist within the failing kidney.

Clinical Implications, Limitations, and Conclusions

RNA-based confirmation of splicing defects enabled reclassification of multiple variants and improved diagnostic interpretation, with direct clinical implications. Moreover, precise delineation of aberrant exon usage nominates potential targets for emerging splice-modifying therapies.[5] This study demonstrates the feasibility of integrating histopathology, ultrastructure, and transcriptomics from archived kidney tissue, enabling molecular diagnosis when DNA-based testing is inconclusive.

Limitations include the retrospective design, incomplete clinical data, and the use of bulk tissue

transcriptomics, which may obscure cell-specific effects. In addition, histopathologic injury markers such as IFTA and glomerulosclerosis represent important potential confounders of the observed expression patterns. As these lesions closely reflect renal functional decline in our cohort, they likely contribute substantially to the transcriptomic differences observed between eGFR-defined groups. Future studies integrating long-read sequencing and single-cell approaches will be essential to resolve unresolved cases and refine molecular interpretation. A further limitation of RNA-based splicing analysis is the potential impact of nonsense-mediated mRNA decay, which selectively degrades transcripts containing premature termination codons. This process may reduce the abundance of aberrantly spliced transcripts and lead to underestimation of splice defects in RNA-seq data. A practical limitation of our study is the requirement for relatively high-quality RNA derived from fresh-frozen tissue. In routine clinical practice, formalin-fixed paraffin-embedded kidney biopsies are more commonly available; however, RNA degradation and chemical modification in formalin-fixed paraffin-embedded samples often limit their suitability for comprehensive transcriptome analysis. Another limitation of this study is the absence of comprehensive genome-wide DNA analysis. Although targeted DNA sequencing was performed to validate RNA-derived variants and assess known disease-associated genes, this approach does not exclude the presence of additional pathogenic variants in other genes or noncoding regions. In particular, digenic inheritance or multilocus contributions may be present in some patients and could influence disease severity and phenotypic variability.

In conclusion, kidney tissue transcriptome sequencing enhances diagnostic yield and biological understanding across the Alport spectrum by revealing splice defects, quantitative exon usage variability, and molecular signatures of renal decline. These findings support integration of RNA sequencing into diagnostic workflows for hereditary nephropathies and provide a framework for functional variant interpretation and therapeutic development.

DISCLOSURE

All the authors declared no competing interests.

ACKNOWLEDGMENTS

This work was supported by the Slovenian Research and Innovation Agency (Research Core Funding No. P3-0054).

DATA AVAILABILITY STATEMENT

GEO accession number: GSE318857.

AUTHOR CONTRIBUTIONS

AZ, NK, and JP conceived and supervised the study. AZ wrote the paper with input from other coauthors. NK, AM, ŽVH, ŠB, and NP performed clinical data evaluation. AZ, ŠK, SP, and AM carried out molecular investigations. NK and JP analyzed the renal biopsies using light and electron microscopy. AZ and ŠK performed the bioinformatics and statistical analyses. All authors have reviewed and approved the final manuscript.

SUPPLEMENTARY MATERIAL

Supplementary file (PDF)

Supplementary Reference.

Supplementary Methods.

Supplementary Tables (xlsx)

Figure S1. Kaplan–Meier estimate of kidney survival in Alport syndrome.

Figure S2. Longitudinal serum creatinine trajectories stratified by gene and gender.

Figure S3. Longitudinal serum creatinine trajectories stratified by detected variant and gender.

Figure S4. Longitudinal eGFR trajectories by type of Alport syndrome.

Figure S5. eGFR trajectories by detected X-linked variant and gender.

Figure S6. eGFR trajectories by genotype status.

Table S1. Clinical, histopathological, and genetic characteristics of the Alport spectrum cohort.

Table S2. Genetic variants identified by whole-transcriptome sequencing, including RNA findings, pathogenicity assessment, and previous DNA testing.

Table S3. Quantification of aberrant splicing events by QSV analysis using adjusted normal-to-skipped transcript peak ratios.

MINSEQE Checklist.

REFERENCES

1. Kashtan C. Alport syndrome: facts and opinions. *F1000Res*. 2017;6:50. https://doi.org/10.12688/f1000research.9636.1
2. Groopman EE, Marasa M, Cameron-Christie S, et al. Diagnostic utility of exome sequencing for kidney disease. *N Engl J Med*. 2019;380:142–151. https://doi.org/10.1056/NEJMoa1806891
3. Savige J. Alport syndrome: an update. *Curr Opin Nephrol Hypertens*. 2025;34:206–211. https://doi.org/10.1097/MNH.0000000000001063
4. Savige J. Understanding better the genetic causes of hematuria. *J Am Soc Nephrol*. 2025;36:4–6. https://doi.org/10.1681/ASN.0000000570
5. Boisson M, Arrondel C, Cagnard N, et al. A wave of deep intronic mutations in X-linked Alport syndrome. *Kidney Int*. 2023;104:367–377. https://doi.org/10.1016/j.kint.2023.05.006
6. Yamamura T, Horinouchi T, Aoto Y, Lennon R, Nozu K. The contribution of COL4A5 splicing variants to the pathogenesis of X-linked Alport syndrome. *Front Med (Lausanne)*. 2022;9:841391. https://doi.org/10.3389/fmed.2022.841391

7. Lord J, Baralle D. Splicing in the diagnosis of rare disease: advances and challenges. *Front Genet*. 2021;12:689892. https://doi.org/10.3389/fgene.2021.689892
8. Cummings BB, Marshall JL, Tukiainen T, et al. Improving genetic diagnosis in Mendelian disease with transcriptome sequencing. *Sci Transl Med*. 2017;9:eaal5209. https://doi.org/10.1126/scitranslmed.aal5209
9. Lake BB, Chen S, Hoshi M, et al. A single-nucleus RNA-sequencing pipeline to decipher the molecular anatomy and pathophysiology of human kidneys. *Nat Commun*. 2019;10:2832. https://doi.org/10.1038/s41467-019-10861-2
10. Garanto A. RNA-Based therapeutic strategies for inherited retinal dystrophies. *Adv Exp Med Biol*. 2019;1185:71–77. https://doi.org/10.1007/978-3-030-27378-1_12
11. Macheroux EP, Braunisch MC, Pucci Pegler S, et al. The hypomorphic variant p.(Gly624Asp) in COL4A5 as a Possible Cause for an Unexpected Severe Phenotype in a Family With X-Linked Alport Syndrome. *Front Pediatr*. 2019;7:485. https://doi.org/10.3389/fped.2019.00485
12. Zurowska AM, Bielska O, Daca-Roszak P, et al. Mild X-linked Alport syndrome due to the COL4A5 G624D variant originating in the Middle Ages is predominant in Central/East Europe and causes kidney failure in midlife. *Kidney Int*. 2021;99:1451–1458. https://doi.org/10.1016/j.kint.2020.10.040
13. Kruger BM, Jens A, Neuhaus A, et al. COL4A5-p.Gly624Asp is the predominant variant in Europe associated with a mild Alport syndrome phenotype. *Kidney Int Rep*. 2025;10:1372–1383. https://doi.org/10.1016/j.ekir.2025.02.031
14. Savige J, Huang M, Croos Dabrera MS, Shukla K, Gibson J. Genotype-phenotype correlations for pathogenic COL4A3-COL4A5 variants in X-linked, autosomal recessive, and autosomal dominant Alport syndrome. *Front Med (Lausanne)*. 2022;9:865034. https://doi.org/10.3389/fmed.2022.865034
15. Barbosa P, Savisaar R, Carmo-Fonseca M, Fonseca A. Computational prediction of human deep intronic variation. *GigaScience*. 2022;12:giad085. https://doi.org/10.1093/gigascience/giad085
16. Murdock DR, Guo DC, DePaolo JS, et al. Non-canonical splice variants in thoracic aortic dissection cases and Marfan syndrome with negative genetic testing. *NPJ Genom Med*. 2025;10:25. https://doi.org/10.1038/s41525-025-00472-w
17. Jung H, Lee KS, Choi JK. Comprehensive characterisation of intronic mis-splicing mutations in human cancers. *Oncogene*. 2021;40:1347–1361. https://doi.org/10.1038/s41388-020-01614-3
18. Qian X, Wang J, Wang M, et al. Identification of deep-intronic splice mutations in a large cohort of patients with inherited retinal diseases. *Front Genet*. 2021;12:647400. https://doi.org/10.3389/fgene.2021.647400
19. Blakes AJM, Wai HA, Davies I, et al. A systematic analysis of splicing variants identifies new diagnoses in the 100,000 Genomes Project. *Genome Med*. 2022;14:79. https://doi.org/10.1186/s13073-022-01087-x
20. Fadaie Z, Khan M, Del Pozo-Valero M, et al. Identification of splice defects due to noncanonical splice site or deep-intronic variants in ABCA4. *Hum Mutat*. 2019;40:2365–2376. https://doi.org/10.1002/humu.23890
21. Truty R, Ouyang K, Rojahn S, et al. Spectrum of splicing variants in disease genes and the ability of RNA analysis to reduce uncertainty in clinical interpretation. *Am J Hum Genet*. 2021;108:696–708. https://doi.org/10.1016/j.ajhg.2021.03.006
22. Wang R, Helbig I, Edmondson AC, Lin L, Xing Y. Splicing defects in rare diseases: transcriptomics and machine learning strategies towards genetic diagnosis. *Brief Bioinform*. 2023;24:bbad284. https://doi.org/10.1093/bib/bbad284
23. Thompson BA, Walters R, Parsons MT, et al. Contribution of mRNA splicing to mismatch repair gene sequence variant interpretation. *Front Genet*. 2020;11:798. https://doi.org/10.3389/fgene.2020.00798
24. Plesko J, Kojc N, Kert S, et al. Severe clinical phenotype in Alport syndrome due to 2 COL4A4 exon-skipping events. *Kidney Med*. 2025;7:101077. https://doi.org/10.1016/j.xkme.2025.101077
25. Tubeuf H, Caputo SM, Sullivan T, et al. Calibration of pathogenicity due to variant-induced leaky splicing defects by using BRCA2 Exon 3 as a model system. *Cancer Res*. 2020;80:3593–3605. https://doi.org/10.1158/0008-5472.CAN-20-0895
26. Danis D, Jacobsen JOB, Carmody LC, et al. Interpretable prioritization of splice variants in diagnostic next-generation sequencing. *Am J Hum Genet*. 2021;108:2205. https://doi.org/10.1016/j.ajhg.2021.09.014
27. Hoberg-Vetti H, Ognedal E, Buisson A, et al. The intronic BRCA1 c.5407-25T>A variant causing partly skipping of exon 23-a likely pathogenic variant with reduced penetrance? *Eur J Hum Genet*. 2020;28:1078–1086. https://doi.org/10.1038/s41431-020-0612-1
28. Lona-Durazo F, Omachi K, Fermin D, et al. Association of genetically predicted skipping of COL4A4 Exon 27 with hematuria and albuminuria. *J Am Soc Nephrol*. 2025;36:48–59. https://doi.org/10.1681/ASN.0000000000000480
29. Gianesello L, Del Prete D, Anglani F, Calò LA. Genetics and phenotypic heterogeneity of Dent disease: the dark side of the moon. *Hum Genet*. 2021;140:401–421. https://doi.org/10.1007/s00439-020-02219-2
30. Arnous MG, Arroyo J, Cogal AG, et al. The site and type of CLCN5 genetic variation impact the resulting dent Disease-1 phenotype. *Kidney Int Rep*. 2023;8:1220–1230. https://doi.org/10.1016/j.ekir.2023.03.012
31. Tosetto E, Ghiggeri GM, Emma F, et al. Phenotypic and genetic heterogeneity in Dent's disease–the results of an Italian collaborative study. *Nephrol Dial Transplant*. 2006;21:2452–2463. https://doi.org/10.1093/ndt/gfl274
32. Riedhammer KM, Braunisch MC, Gunthner R, et al. Exome sequencing and identification of phenocopies in patients with clinically presumed hereditary nephropathies. *Am J Kidney Dis*. 2020;76:460–470. https://doi.org/10.1053/j.ajkd.2019.12.008
33. Wopperer FJ, Knaup KX, Stanzick KJ, et al. Diverse molecular causes of unsolved autosomal dominant tubulointerstitial kidney diseases. *Kidney Int*. 2022;102:405–420. https://doi.org/10.1016/j.kint.2022.04.031
34. Loderbauer L, Knaup KX, Reisenbuchler D, et al. Alport syndrome is a partial tubulointerstitial disease of the kidney. *Kidney Int Rep*. 2026;11:103694. https://doi.org/10.1016/j.ekir.2025.11.019
35. Sureshbabu A, Muhsin SA, Choi ME. TGF-beta signaling in the kidney: profibrotic and protective effects. *Am J Physiol Ren Physiol*. 2016;310:F596–F606. https://doi.org/10.1152/ajprenal.00365.2015

36. Rudman-Melnick V, Adam M, Potter A, et al. Single-cell profiling of AKI in a murine model reveals novel transcriptional signatures, profibrotic phenotype, and epithelial-to-stromal crosstalk. *J Am Soc Nephrol*. 2020;31:2793–2814. https://doi.org/10.1681/ASN.2020010052

37. Lu YA, Liao CT, Raybould R, et al. Single-nucleus RNA sequencing identifies new classes of proximal tubular epithelial cells in kidney fibrosis. *J Am Soc Nephrol*. 2021;32:2501–2516. https://doi.org/10.1681/ASN.2020081143

38. Wen Y, Su E, Xu L, et al. Analysis of the human kidney transcriptome and plasma proteome identifies markers of proximal tubule maladaptation to injury. *Sci Transl Med*. 2023;15:eade7287. https://doi.org/10.1126/scitranslmed.ade7287

39. Reck M, Baird DP, Veizades S, et al. Multiomic analysis of human kidney disease identifies a tractable inflammatory and pro-fibrotic tubular cell phenotype. *Nat Commun*. 2025;16:4745. https://doi.org/10.1038/s41467-025-59997-4

40. Abedini A, Levinsohn J, Klotzer KA, et al. Single-cell multi-omic and spatial profiling of human kidneys implicates the fibrotic microenvironment in kidney disease progression. *Nat Genet*. 2024;56:1712–1724. https://doi.org/10.1038/s41588-024-01802-x

41. Li H, Dixon EE, Wu H, Humphreys BD. Comprehensive single-cell transcriptional profiling defines shared and unique epithelial injury responses during kidney fibrosis. *Cell Metab*. 2022;34:1977–1998. e1979 https://doi.org/10.1016/j.cmet.2022.09.026

42. Hinze C, Kocks C, Leiz J, et al. Single-cell transcriptomics reveals common epithelial response patterns in human acute kidney injury. *Genome Med*. 2022;14:103. https://doi.org/10.1186/s13073-022-01108-9

43. Lake BB, Menon R, Winfree S, et al. An atlas of healthy and injured cell states and niches in the human kidney. *Nature*. 2023;619:585–594. https://doi.org/10.1038/s41586-023-05769-3

44. Sun J, Wang J, Lu W, et al. MiR-325-3p inhibits renal inflammation and fibrosis by targeting CCL19 in diabetic nephropathy. *Clin Exp Pharmacol Physiol*. 2020;47:1850–1860. https://doi.org/10.1111/1440-1681.13371

45. Qiu Z, Zhong Z, Zhang Y, Tan H, Deng B, Meng G. Human umbilical cord mesenchymal stem cell-derived exosomal miR-335-5p attenuates the inflammation and tubular epithelial-myofibroblast transdifferentiation of renal tubular epithelial cells by reducing ADAM19 protein levels. *Stem Cell Res Ther*. 2022;13:373. https://doi.org/10.1186/s13287-022-03071-z

46. Du W, Tang H, Lei Z, et al. miR-335-5p inhibits TGF-beta1-induced epithelial-mesenchymal transition in non-small cell lung cancer via ROCK1. *Respir Res*. 2019;20:225. https://doi.org/10.1186/s12931-019-1184-x

47. Dai Y, Gao M, Li L, et al. MicroRNA-874-3p aggravates doxorubicin-induced renal podocyte injury via targeting methionine sulfoxide reductase B3. *Oxid Med Cell Longev*. 2020;2020:9481841. https://doi.org/10.1155/2020/9481841